Applied Physics B (2023) 129:50
https://doi.org/10.1007/s00340-023-07994-0

Applied Physics B
Lasers and Optics

RESEARCH

Clusters of rotating beams with autofocusing and transformation properties generated by a spatial light modulator

Svetlana N. Khonina[1,2] · Alexey P. Porfirev[1,2]

Received: 26 March 2022 / Accepted: 23 February 2023 / Published online: 13 March 2023

Abstract
We theoretically, numerically, and experimentally investigate new types of laser beams with autofocusing, rotating and/or transformation properties. A spatial light modulator generates these laser beams as clusters/sets of shifted vortex Laguerre-Gaussian beams and their superpositions with additional phase distribution. We demonstrate the formation of the clusters of rotating beams with controlled individual autofocusing trajectories as well as different transformations (topological/positional and interference redistribution) and rotation of the entire clusters as complex structures. Moreover, we investigate the possibility of astigmatic transformation of the propagating laser beams clusters. Thus, the proposed techniques provide additional control of the three-dimensional trajectories of the structured laser beams with predetermined intensity and phase distributions and can be used in laser manipulation, laser material processing, and optical microscopy.

1 Introduction

Today, spatial light modulators (SLMs) [1, 2] as a tool for the realization of computer-generated holograms (CGHs) provide a wide range of opportunities for three-dimensional control of structured laser beams in laser material processing [3–6], optical trapping and manipulation [7–9], optical communications [10–12], optical microscopy [13–15], optical imaging [16, 17], etc. [18].

SLMs allow one to shape light fields with the desired distribution of amplitude, phase, or polarization state as well as to simultaneously control all three mentioned characteristics for the generation of vector fields with different features [19–21]. Although SLMs can manipulate light by modulating the amplitude, phase, or polarization of the light fields in the two dimensions of space and time, most of the SLMs are phase-only elements, which are mainly used to shape the spatial phase distribution of the light beam directly without touching the amplitude distribution [22]. In this case, such algorithms as the Gerchberg-Saxton algorithm [23] and its modifications [24, 25] are widely used for the design phase diffractive optical elements (DOEs) generating predetermined amplitude distributions. The amplitude encoding techniques give the possibility to additionally control the phase distribution of the generated light fields [26]. Also, different interferometrical methods using both one and two pure-phase SLMs allow one to tailor polarization distribution and generate vector beams [27, 28].

Such a wide spectrum of approaches of the generation of structured radiation with SLMs led to the demonstration of the SLM-based generation of laser beams with such properties as non-diffraction, rotation during propagation, propagation along curved trajectories, and autofocusing.

Among various structured beams, beams with autofocusing properties are of considerable interest to researchers [29–31]. Such interest is associated with the application of autofocusing beams in various fields, such as optical manipulation [32, 33], multiphoton polymerization [34], nonlinear effects [35], polarization conversion [36], and sharp focusing [37].

The formation of beams with abrupt autofocusing is based on the use of accelerating beams with a nonlinear propagation trajectory, such as the Airy and Pearcey beams [38–40], which are well known from the catastrophe theory [41, 42]. It is also possible to form other beams with arbitrary trajectories or caustics [43, 44]. Note, the abrupt autofocusing is provided by mirror or circular symmetrization of accelerating beams [45–48].

✉ Svetlana N. Khonina
khonina@ipsiras.ru

1 IPSI RAS-Branch of the FSRC “Crystallography and Photonics” RAS, Molodogvardeyskaya St. 151, 443001 Samara, Russia

2 Samara National Research University, Moskovskoe Shosse, 34, 443086 Samara, Russia

The demand for autofocusing beams in various applications stimulates scientists to search for new modifications and generalizations of such beams [49–52]. One of the approaches to expanding the types and diversity of the structure of autofocusing beams is the formation of sets or clusters of different shifted beams [53–56].

Note that clusters of shifted Gaussian or Laguerre-Gaussian (LG) beams [53, 54, 56] demonstrate linear (i.e. without acceleration) propagation trajectories. However, clusters of shifted Airy beams with acceleration propagation properties can demonstrate more complex 3D propagation scenarios [55].

An additional degree of freedom for controlling the 3D trajectory is the additional individual deflecting phase (spatial carriers) to each cluster's beam [48, 56]. For example, in [56], rotating clusters of LG beams were formed due to such deflecting phases. Note, however, that the intensity of each LG beam in the cluster did not rotate. In this paper, we expand the types of beams under consideration, so we use in clusters various superpositions of LG beams, including those whose intensity rotates during propagation. Thus, it is possible to form not only clusters rotating as whole structures, but also ensure the rotation of their individual components, which expands the range of beams used for optical trapping and manipulation.

Moreover, we consider another approach, when a set of shifted beams is supplemented by a common phase function that ensures a change in the propagation trajectory of the entire cluster. We considered functions with a power-law dependence on the radius, including a linear one, which corresponds to a diffractive axicon. In this case, it is possible not only to change the propagation trajectory of cluster's beams, but also their additional transformations, such as topological/positional and interference redistribution, and also astigmatic distortion. In particular, a diffractive axicon [57–59], which in binary form is a ring grating [60, 61], can be used for astigmatic transformation of beams [62] which makes it possible to measure the orbital angular momentum (OAM) of vortex beams [63, 64].

For numerical simulation, the fractional Fourier transform (FrFT) [65–67] was used, which describes the propagation of beams in lens systems [68], in media with a gradient refractive index [69], and also in nonlocal nonlinear media [70, 71].

Both approaches were experimentally implemented using a SLM, which makes it possible to dynamically control the 3D structure of the formed beams by changing both the propagation trajectory and the distribution of the transverse intensity of each cluster's element during propagation.

2 Theoretical background

To simulate the propagation of light beams, we use the fractional Fourier transform [65–67]:

$$G(u,v,z) = -\frac{ik}{2\pi f \sin(\tau z)} \exp\left\{\frac{ik\left(u^2+v^2\right)}{2f\tan(\tau z)}\right\} \iint\limits_D g(x,y)\exp\left[\frac{ik\left(u^2+v^2\right)}{2f\tan(\tau z)} - \frac{ik(xu+yv)}{f\sin(\tau z)}\right] \mathrm{d}x\mathrm{d}y, \tag{1}$$

where $k = 2\pi/\lambda$, λ is the light wavelength, f is the focal length of a lens, $\tau = \pi/(2f)$, z is the distance from the input plane, D is the aperture domain in the input plane, (x,y) and (u,v) are transverse coordinates in the input and output plane, accordingly.

Expression (1) is a convenient tool for modeling field $g(x, y)$ propagation after a focusing lens.

First, we consider the field in the input plane ($z=0$) as a set of shifted light beams $\Psi_p(x, y)$:

$$g(x,y) = \sum_{p=1}^{P} c_p \Psi_p\left(x - x_p, y - y_p\right), \tag{2}$$

where c_p are complex coefficients, $\left(x_p, y_p\right)$ are displacement coordinates.

In this paper, as beams $\Psi_p(x, y)$, we consider various superpositions of LG modes [72]:

$$LG_{nm}(r,\varphi) = A_{nm}\exp\left(-\frac{r^2}{\sigma_0^2}\right)\cdot\left(\frac{\sqrt{2}r}{\sigma_0}\right)^{|m|} L_n^{|m|}\left(\frac{2r^2}{\sigma_0^2}\right)\exp(im\varphi), \tag{3}$$

where (r, φ) are polar coordinates, $L_n^m(x)$ is the generalized Laguerre polynomial, σ_0 is the radius of the Gaussian beam in the input plane, A_{nm} is the normalization coefficient.

It is known that LG beams are modes of resonators [73], gradient media [69] and demonstrate invariance up to scale when propagating in free space and passing through lens systems [74–76].

In particular, the LG mode defined by Eq. (3) when propagating in free space at a distance z takes the following form:

$$LG_{nm}(r,\varphi,z) = A_{nm}\exp\left[i\frac{2\pi}{\lambda}z + \frac{i\pi r^2}{\lambda R(z)} - \frac{r^2}{\sigma^2(z)}\right]\left(\frac{\sqrt{2}r}{\sigma(z)}\right)^{|m|} L_n^{|m|}\left(\frac{2r^2}{\sigma^2(z)}\right)\exp\left[-i\beta_{nm}(z) + im\varphi\right], \tag{4}$$

where $\sigma^2(z) = \sigma_0^2\left(1 + z^2/z_0^2\right)$ is the effective beam radius, $z_0 = \pi\sigma_0^2/\lambda$ is the confocal parameter, $\beta_{nm}(z) = (2n+m+1)arctg\left(z/z_0\right)$, $R(z) = z\left(1 + z_0^2/z^2\right)$ is the radius of curvature of the parabolic front of the light field.

When the LG mode defined by Eq. (3) is focused by a lens with focal length f, the following distribution will be in the focal plane:

$$LG_{nm}(r,\varphi,f) = (-1)^n i^{|m|} A_{nm} \exp\left(-\frac{r^2}{\sigma_f^2}\right) \cdot \left(\frac{\sqrt{2}r}{\sigma_f}\right)^{|m|} L_n^{|m|}\left(\frac{2r^2}{\sigma_f^2}\right) \exp(im\varphi), \tag{5}$$

where $\sigma_f = \lambda f / (\pi\sigma_0)$ is the effective beam radius in the focal plane.

As can be seen from Eqs. (4) and (5), the intensity distribution of LG modes is preserved on a scale. However, this is only true for single LG modes. If the beam contains a superposition of LG modes, then the intensity pattern of the beam will change during propagation depending on the mode indices in the superposition:

$$\Psi(x,y) = \sum_{n,m\in\Omega} b_{nm} LG_{nm}(r,\varphi), \tag{6}$$

where b_{nm} are complex coefficients, Ω is the set of indices.

The intensity of the beam defined by Eq. (6) at different distances z has the following form:

$$|\Psi(x,y,z)|^2 = \sum_{n,m\in\Omega} \left|b_{nm}\right|^2 \left|LG_{nm}(r,\varphi,z)\right|^2 + 2\sum_{n\neq n',m\neq m'} \left|b_{nm}b_{n'm'}\right| \cdot \left|LG_{nm}(r,\varphi,z) LG_{n'm'}(r,\varphi,z)\right| \cdot \cos\Phi_{n'm'}^{nm}(r,\varphi,z), \tag{7}$$

where

$$\Phi_{n'm'}^{nm}(r,\varphi,z) = \arg b_{nm} - \arg b_{n'm'} + \left[2(n-n') + (|m| - |m'|)\right] arctg\left(z/z_0\right) + \left(m-m'\right)\varphi. \tag{8}$$

It was shown in [75, 76] that by imposing special conditions on the set of indices Ω in Eq. (6), it is possible to form beams with different properties, including an invariant and rotating intensity distribution during propagation. In particular, the rotation condition for a multimode beam defined by Eq. (6) has the following form:

$$\Omega: \frac{2(n-n') + (|m| - |m'|)}{m-m'} = const. \tag{9}$$

Note that expressions (7)–(8) describe the propagation of superposition LG modes defined by Eq. (6) along the optical axis. When the beam defined by Eq. (6) is displaced in the input plane in accordance with Eq. (2), the propagation trajectory will change, however, the rotational nature of the beam as a whole will remain, since each mode in superposition defined by Eq. (6) travels the same distance.

A similar result will be obtained when each shifted beam is supplemented with a deflecting phase (spatial carriers). However, in this case, the formation of more complex propagation trajectories is possible [48, 56]

More complex transformations of individual beams in a cluster will occur if a common phase function is introduced in the input plane with a power-law dependence on the radius:

$$g_{ch}(x,y) = \exp\left[i(k\alpha r)^q\right] \sum_{p=1}^{P} c_p \Psi_p\left(x-x_p, y-y_p\right), \tag{10}$$

where $r = \sqrt{x^2+y^2}$, α is a dimensionless parameter.

Note that additional radial phase functions $\exp\left[i(k\alpha r)^q\right]$ were used to generate autofocusing chirp-beams [77] and aberration beams [51].

In this paper, we consider two types of such functions for $1 \le q < 1$, which corresponds to sublinear chirp [30, 37, 51] ($q = 1$ for a diffractive axicon), and $q > 2$, which corresponds to superlinear chirp [77].

Next, using Eq. (1), we study in detail various properties of shifted beams of the form defined by Eqs. (2) and (10).

3 Analysis and simulation results

3.1 Clusters of shifted beams with deflecting phases (spatial carriers)

Let us consider a set of beams defined by Eq. (2) displaced from the center in the input plane. The propagation of such a set of beams using operator defined by Eq. (1) is described as follows:

$$G(u,v,z) = -\frac{ik}{2\pi f \sin(\tau z)} \exp\left\{\frac{ik\left(u^2+v^2\right)}{2f\tan(\tau z)}\right\} \times \sum_{p=1}^{P} c_p(z) \iint_D \Psi_p(x,y) \exp\left[\frac{ik\left(u^2+v^2\right)}{2f\tan(\tau z)} - \frac{ik(xu+yv)}{f\sin(\tau z)}\right] dxdy, \tag{11}$$

where

$$c_p(z) = c_p \exp\left[-\frac{ik\left(x_p u + y_p v\right)}{f\sin(\tau z)}\right], \tag{12}$$

As can be seen from Eqs. (11), (12), each beam of the set acquires an additional phase shift $\exp\left[-\frac{ik\left(x_p u+y_p v\right)}{f\sin(\tau z)}\right]$ in accordance with the displacement coordinates $\left(x_p, y_p\right)$ and the distance traveled z. Thus, by changing the displacement parameters $\left(x_p, y_p\right)$, one can actually control the phase of the coefficients c_p, which determines the interference pattern in different planes as cluster's beams propagate.

In addition, it is possible to change the beam's propagation trajectory by supplementing each cluster's beam with a deflecting phase (spatial carriers) $s_p(x, y)$:

$$g(x,y) = \sum_{p=1}^{P} c_p \Psi_p\left(x - x_p, y - y_p\right) s_p(x,y), \tag{13}$$

where

$$s_p(x,y) = \exp\left[ik\left(s_{px}x + s_{py}y\right)\right], \tag{14}$$

where s_{px}, s_{py} are dimensionless parameters corresponding to spatial carrier frequencies.

Then the propagation of a set of beams of Eq. (13) is described as follows:

$$G(u,v,z) = -\frac{ik}{2\pi f \sin(\tau z)} \exp\left\{\frac{ik\left(u^2+v^2\right)}{2f\tan(\tau z)}\right\} \sum_{p=1}^{P} c_p(z)\cdot G_p\left(u-u_p(z), v-v_p(z)\right), \tag{15}$$

where

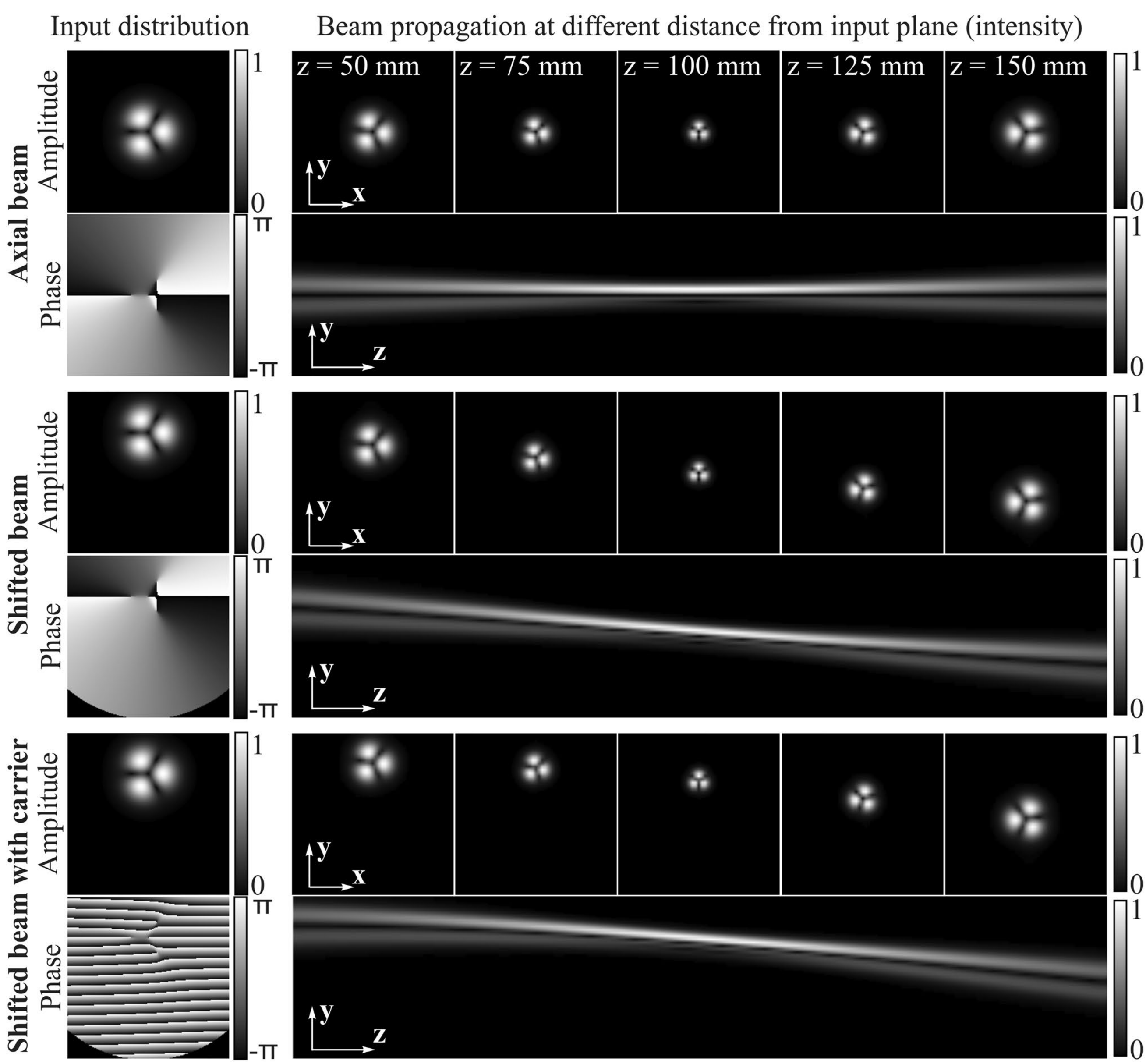

Fig. 1 Simulation results of two-mode LG beam with Ω: $(n_1, m_1) = (0, 1)$, $(n_2, m_2) = (0, -2)$

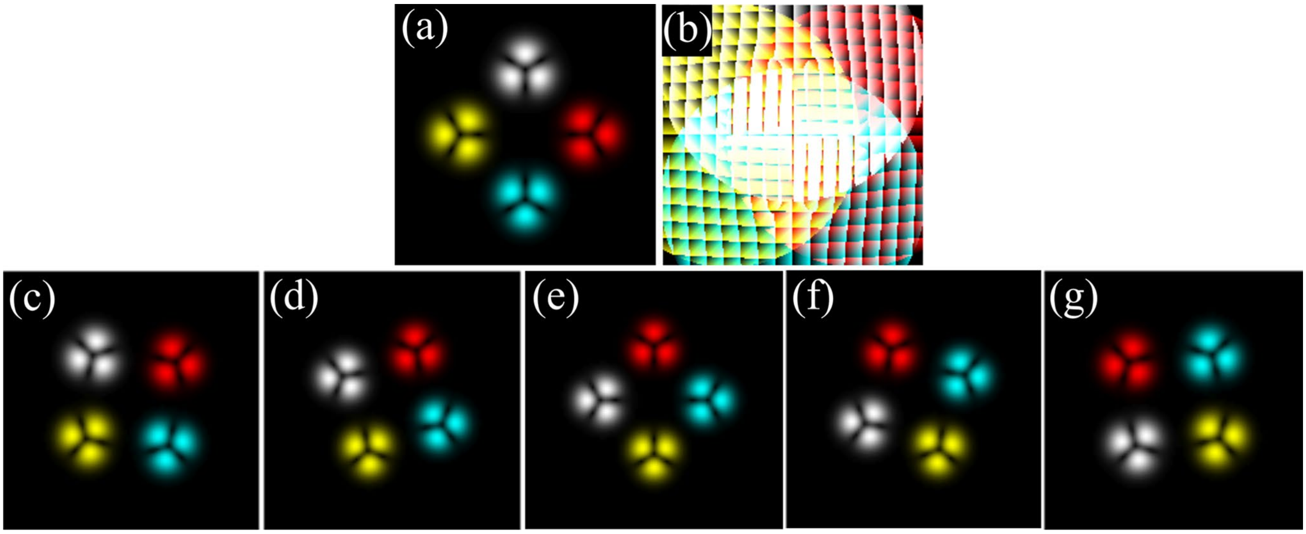

Fig. 2 A quadric of shifted rotated two-mode LG beam with Ω:$(n_1, m_1) = (0, 1)$, $(n_2, m_2) = (0, -2)$ with individual carriers: input **a** amplitude and **b** phase; intensity at different distance from input plane: **c** $z = 50$ mm, **d** $z = 75$ mm, **e** $z = 100$ mm, **f** $z = 125$ mm, **g** $z = 150$ mm (each individual beam of the cluster is specially colored).

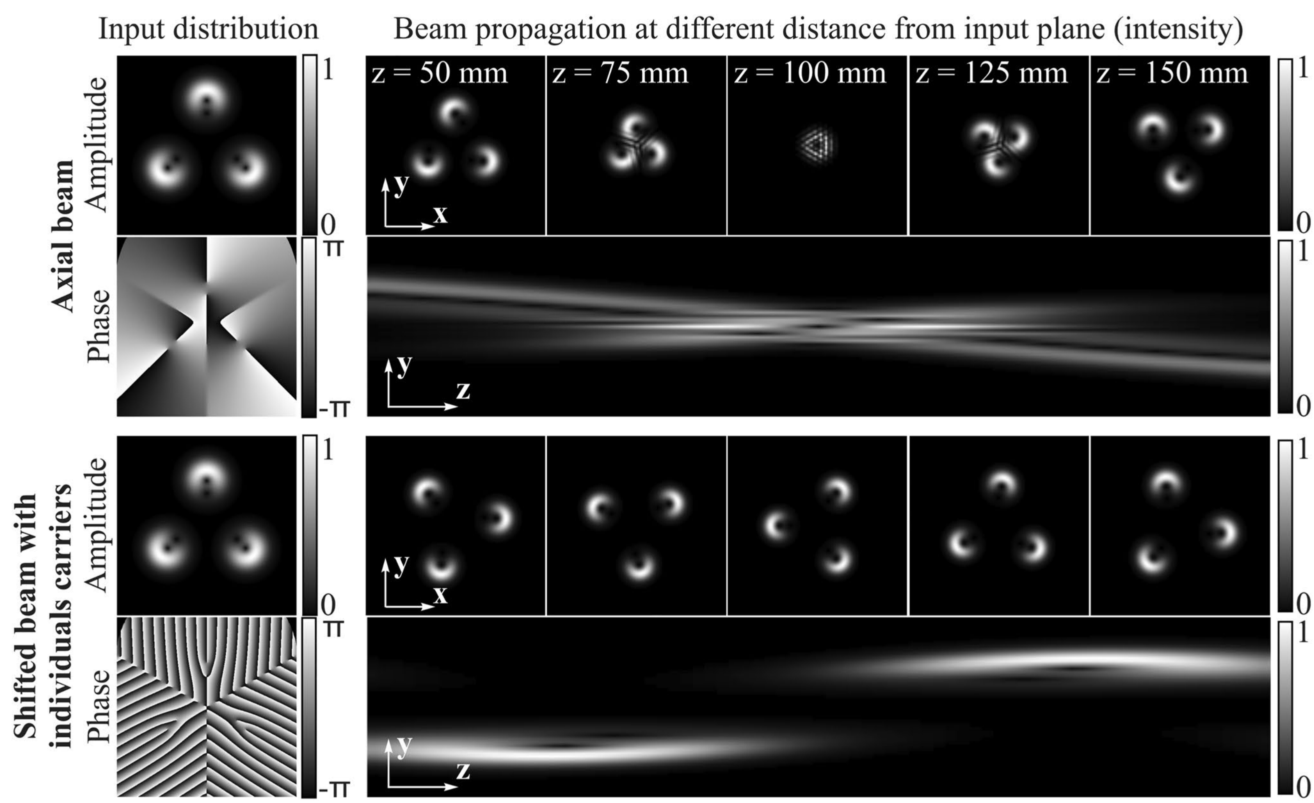

Fig. 3 Simulation results for a triple of two-mode LG beams with Ω: $(n_1, m_1) = (0, 1)$, $(n_2, m_2) = (0, 2)$

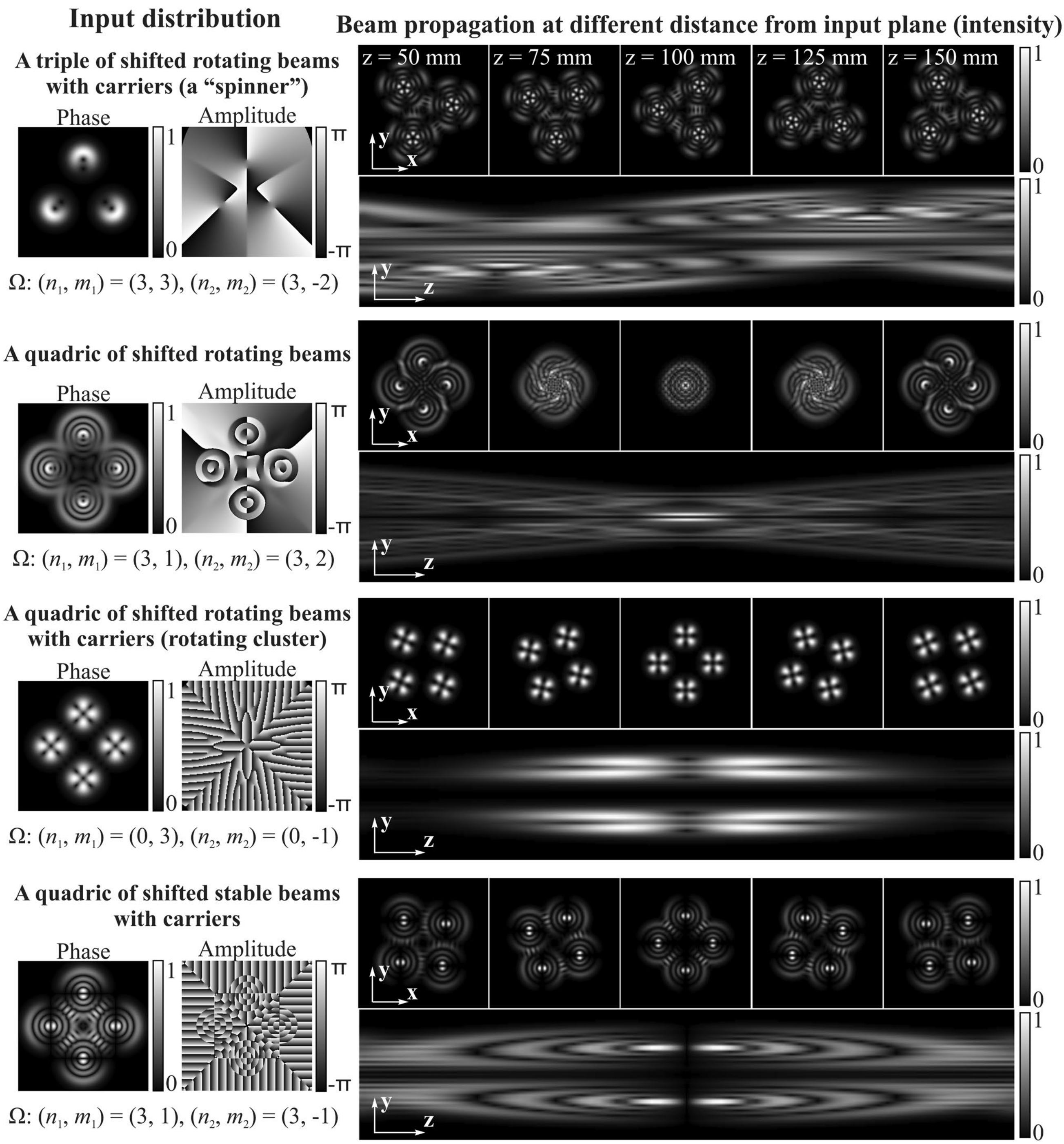

Fig. 4 Simulation results for clusters of superposition LG beams

$$G_p\left(u-u_p(z),v-v_p(z)\right) = \iint_D \Psi_p(x,y)\exp\left[\frac{ik\left(u^2+v^2\right)}{2f\tan(\tau z)} - \frac{ik\left[x\left(u-u_p(z)\right)+y\left(v-v_p(z)\right)\right]}{f\sin(\tau z)}\right]\mathrm{d}x\mathrm{d}y, \tag{16}$$

where $u_p(z) = s_{px} f\sin(\tau z)$, $v_p(z) = s_{py} f\sin(\tau z)$.

Figure 1 shows the results of a comparative simulation of the propagation of a rotating two-mode LG beam defined by Eq. (6) with indices $\Omega: (n_1, m_1) = (0, 1), (n_2, m_2) = (0, -2)$ in the presence of a displacement and a deflecting phase. The following parameters were used for modeling: wavelength $\lambda = 532$ nm, input field size is 2 mm × 2 mm, focal length $f = 100$ mm.

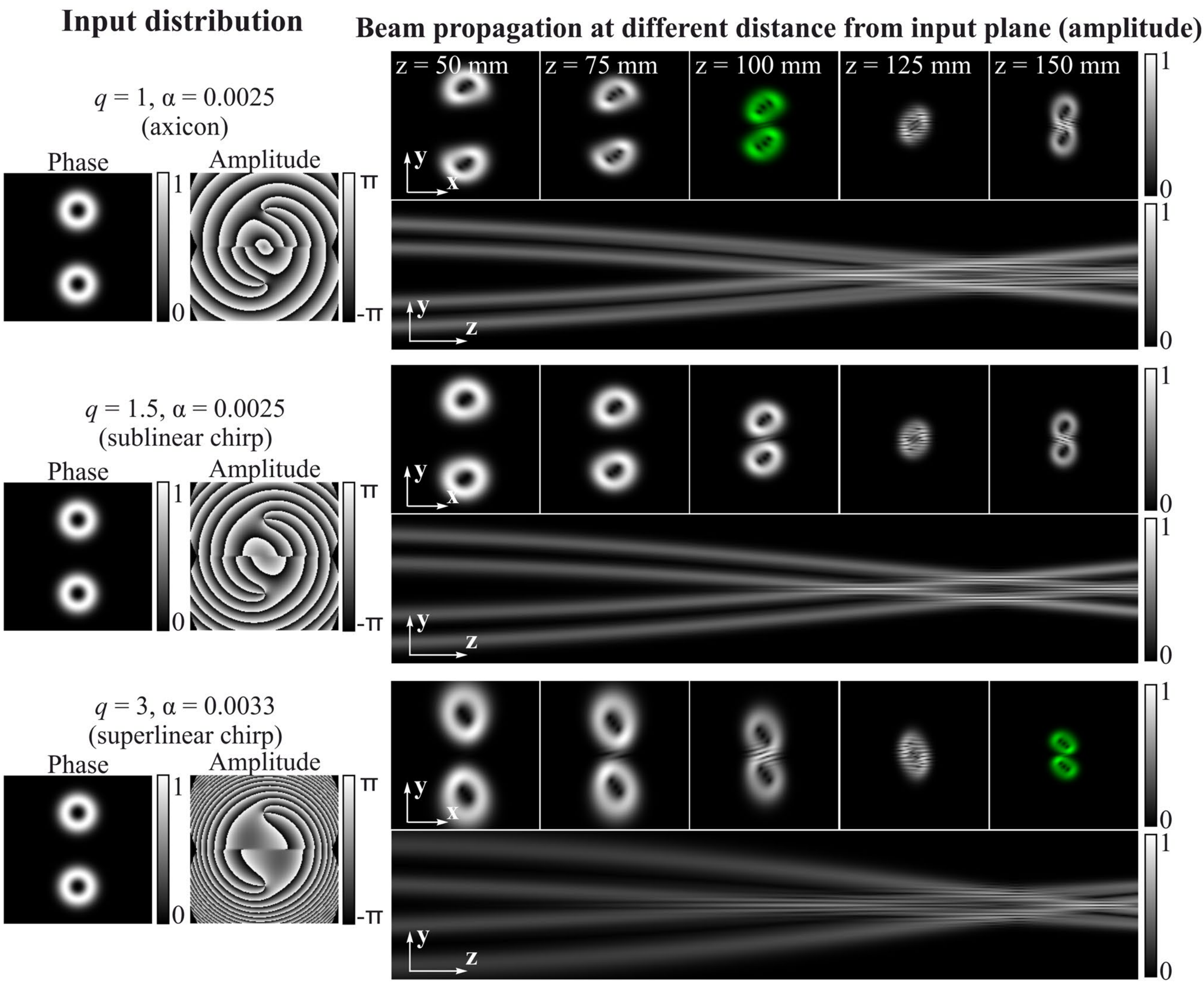

Fig. 5 Simulation results for propagation and transformation of a couple of shifted vortex LG beams $(n, m) = (0, 3)$

As can be seen from the results shown in Fig. 1, when the rotating beam is shifted (the second row of Fig. 1) or/and a deflecting phase is added (the third row of Fig. 1), only the beam's propagation trajectory changes compared with the axial propagation (the first row of Fig. 1). The dynamics of rotation is preserved. This property makes it possible to form various clusters from rotating beams with controlled rearrangement of the cluster configuration during propagation.

Figure 2 shows the propagation simulation results for a cluster of four shifted rotating two-mode LG beams defined by Eq. (6) with indices $\Omega: (n_1, m_1) = (0, 1), (n_2, m_2) = (0, -2)$ in the presence of individual deflecting phases for each cluster's beam. We highlighted each cluster's beam in a separate color to show not only the rotation of the cluster as a whole, but also of each of its components.

Thus, Fig. 2 clearly shows that the change in the structure of the cluster (its rotation as a whole) is achieved by introducing deflecting phases defined by Eq. (13) [shown in Fig. 2(b)], which allow one to control the trajectory of each individual beam in the cluster. This approach is similar to the methods considered earlier in [48, 56]. However, in these works, the intensity of each individual beam in the cluster was not rotated. In this paper, we have extended the types of cluster's beams due to various superpositions of LG beams defined by Eq. (6), including beams with intensity rotates during propagation in accordance with the condition defined by Eq. (9).

Figures 3 and 4 show various examples of clusters of different LG beams defined by Eq. (6).

Figure 3 shows the results of a comparative simulation of the propagation of a triple of shifted rotating two-mode LG beams with indices $\Omega: (n_1, m_1) = (0, 1), (n_2, m_2) = (0, 2)$ without (the first row of Fig. 3) and with the presence of deflecting phases (the second row of Fig. 3) for each beam in the cluster.

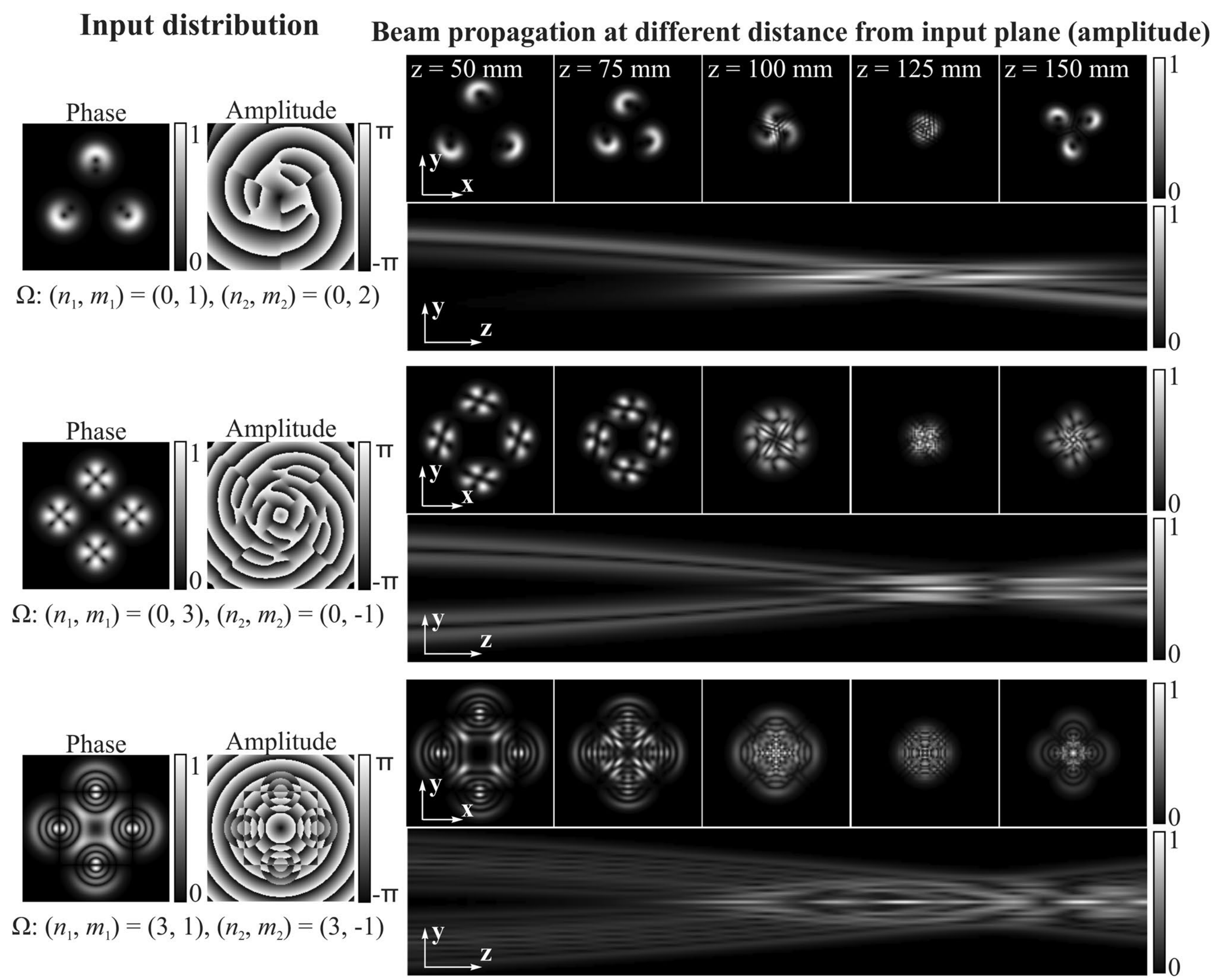

Fig. 6 Simulation results for propagation and transformation clusters with shifted composed LG beams with additional axicon [$q=1$, $\alpha=0.0025$ in Eq. (10)]

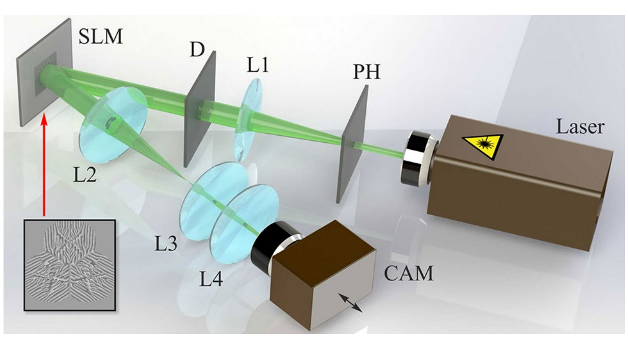

Fig. 7 Experimental setup for the investigation of the designed rotating and autofocusing laser beams: Laser is a solid-state laser, PH is a pinhole (aperture size of 40 µm); L1, L2, L3, and L4 are lenses ($f_1=250$, $f_2=500$, $f_3=150$ mm, and $f_4=150$ mm, respectively), D is a circular aperture, SLM is a spatial light modulator (HOLOEYE, PLUTO VIS with a 1920×1080 pixel resolution), and CAM is a video camera (TOUPCAM UHCCD00800KPA, 3264×2448 pixels)

As can be seen from the comparative results given in Fig. 3, the presence of individual carriers (deflecting phases) in each cluster's beam makes it possible to control the 3D rotating dynamics of the cluster configuration during propagation. This property can be in demand in 3D imaging where rotating point spread functions (PSFs) are used to 3D tracking of fluorescent microparticles in microscopy [78–80].

Thus, it is possible to form not only clusters rotating as a whole, but also ensure the rotation of their individual components, which expands the range of beams used for optical trapping and manipulation of microparticles, laser material processing, and optical microscopy.

3.2 Clusters of shifted beams with transformations at propagating

In the previous section, we considered clusters of shifted beams with individual deflecting phases (spatial carriers) that allow one to control the trajectory of each cluster's component.

In this section, we consider a different approach, when a set of displaced beams is supplemented in the input plane by a common phase function defined by Eq. (10) that ensures a change in the propagation trajectory of the entire cluster.

Moreover, in this case, it is possible provide additional transformations of cluster's beams. In particular, for $q=1$ in Eq. (10), the total complementary phase function corresponds to a diffractive axicon, which was used in [62] for the astigmatic transformation of vortex beams in order to measure OAM.

In this paper, we consider the possibility of using for this purpose not only the diffractive axicon ($q=1$), but also other phase functions, in particular, $q=1.5$ and $q=3$ in Eq. (10).

Figure 5 shows the results of a comparative simulation of the propagation and transformation of a couple of shifted vortex LG beams (n, m) = $(0, 3)$ whose OAM value is proportional to the value of the topological charge (TC) $m=3$ [63, 64].

As can be seen from the results given in Fig. 5, in all cases there is an astigmatic transformation of the vortex beams. Note that the focusing plane shifts from $z=100$ mm to $z=125$ mm because the input field is supplemented by a scattering chirped phase function. This shift is controlled by the parameter α, which was chosen so that in the considered cases the plane of focus shifted by approximately the same distance.

Note that for $1 \le q < 2$ (sublinear chirp) and $q > 2$ (superlinear chirp) the nature of the astigmatic transformation before and after the new focusing plane is different. The astigmatic intensity patterns which make it possible to unambiguously determine the beam's TC $m=3$ (equal to the number of zero lines) [62, 81, 82] are most clearly observed for $q=1$ at $z=100$ mm (the first row of Fig. 5, highlighted in green color, i.e. before the new focal plane), and for $q=3$ at $z=150$ mm (the third row of Fig. 5, highlighted in green color, i.e. after the new focal plane). At $q=1.5$, the astigmatic transformation is insufficient.

The possibility of simultaneously changing the trajectory and transforming the intensity of cluster's beams during propagation due to the common phase function provides diversity of the 3D structures of the considered beams. Some examples are shown in Fig. 6.

As can be seen from the comparison of the simulation results presented in Figs. 3, 4 and 6, the autofocusing dynamics of the clusters with shifted beams and the transverse intensity distribution are significantly different for the two considered approaches.

In the first approach (Sect. 3.1), when each individual cluster's beam is supplemented with individual deflecting phases (spatial carriers), the structure of these beams is preserved during propagation (Figs. 3, 4).

In the second approach (Sect. 3.2), when the entire cluster is completed by a chirped phase, in addition to changing the trajectory, an astigmatic transformation of each individual element of the cluster occurs (Fig. 6).

Both approaches can be implemented using SLM, which will make it possible to dynamically control the 3D structure

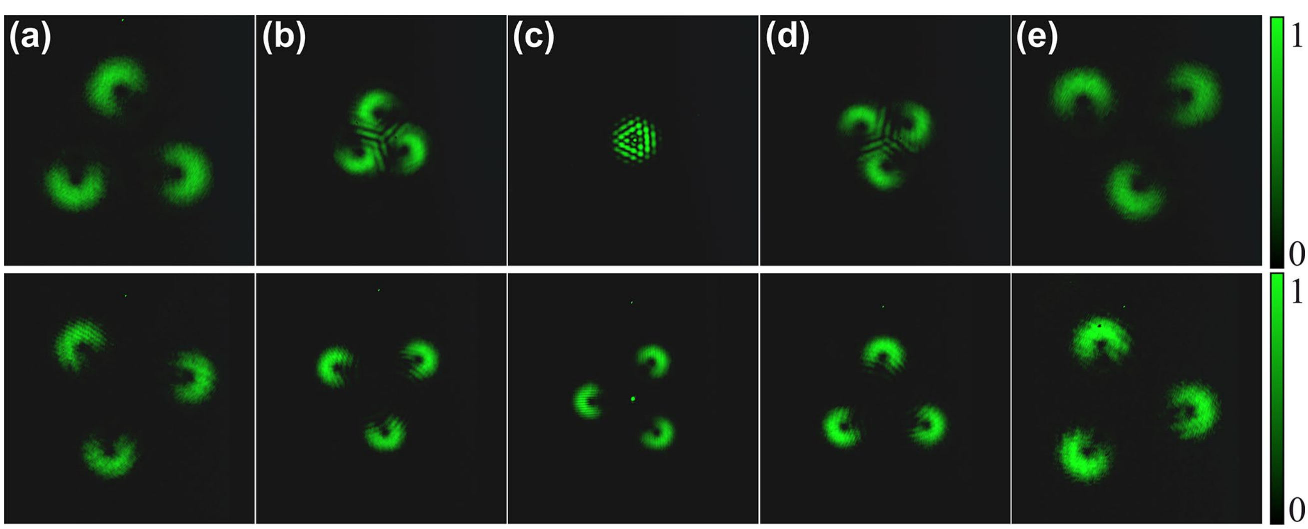

Fig. 8 The intensity distributions of laser beams formed in the case of the triple of two-mode LG beams with Ω: (n_1, m_1) = $(0, 1)$, (n_2, m_2) = $(0, 2)$ at different distances from the plane of the lens L4: **a** f—50 mm, **b** f—25 mm, **c** the focal plane, f, **d** f+50 mm, **e** f+50 mm. The top row shows the distributions for shifted beams and the bottom row—for shifted beams with individual carriers

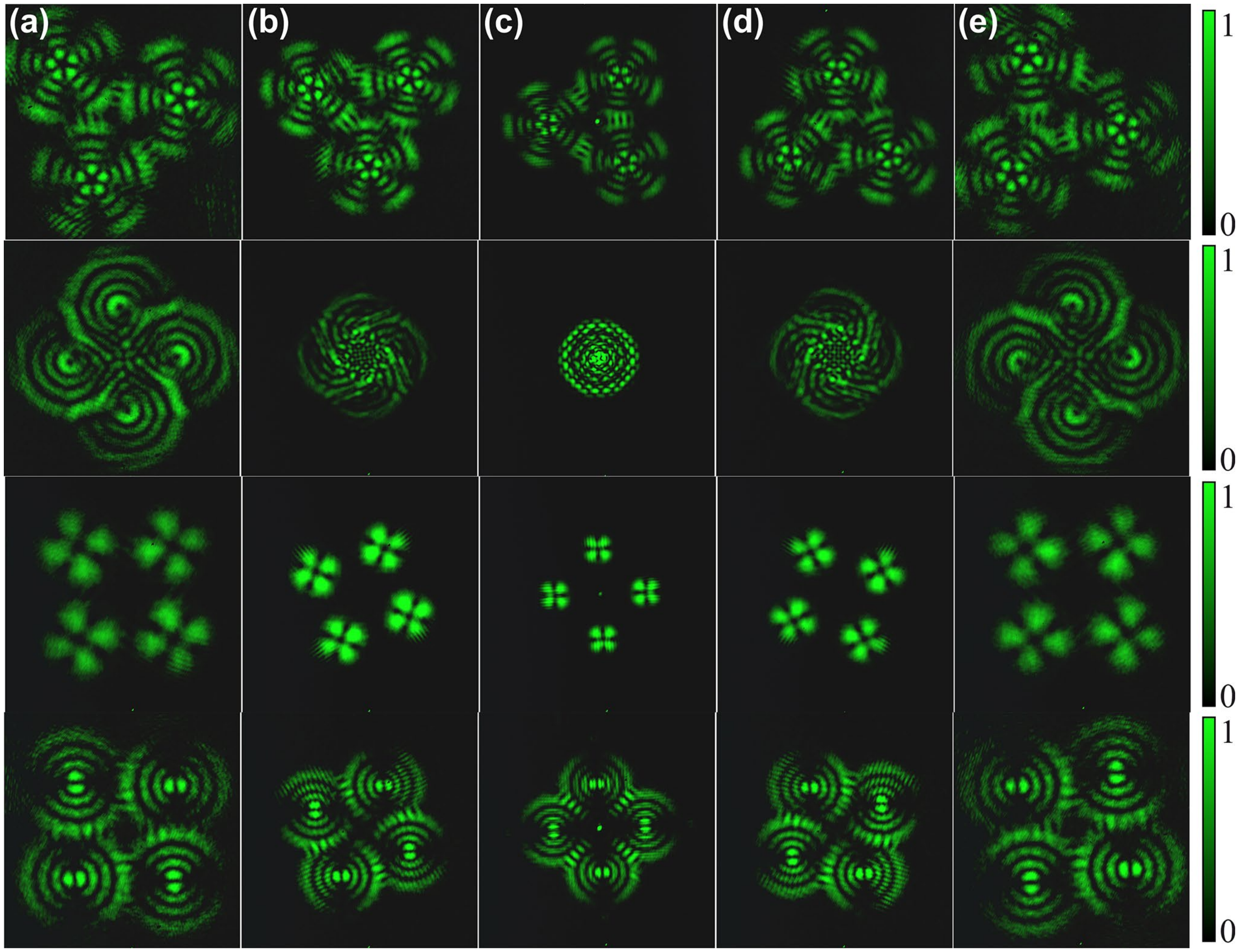

Fig. 9 The intensity distributions of laser beams formed in the case of clusters of superposition LG beams at different distances from the plane of the lens L4: **a** *f*—50 mm, **b** *f*—25 mm, **c** the focal plane, *f*, **d** *f* + 50 mm, **e** *f* + 50 mm. The distributions for triple of shifted rotating beams with carriers (a "spinner"), a quadric of shifted rotating beams, a quadric of shifted rotating beams with carriers (rotating cluster), and a quadric of shifted stable beams with carriers are shown from the top row to the bottom row

of the formed beams by changing both the propagation trajectory and the distribution of the transverse intensity of each cluster's element during propagation.

4 Experimental results

For the investigation of the designed rotating and autofocusing laser beams, we used pure phase masks with encoded complex amplitude distributions [83] and realized with a reflective SLM PLUTO VIS (1920 × 1080 pixel resolution, 8 µm pixel pitch).

The experimental optical setup is shown in Fig. 7. The output laser beam of solid-state laser (λ = 532 nm) was expanded with a system composed of a pinhole PH (aperture size of 40 µm) and a lens L1 (f_1 = 250 mm) to illuminate the SLM. A diaphragm D was used to separate the central spot of the Airy disk resulting from the wave diffraction of the pinhole. Then, after the SLM with the encoded phase masks, lenses L2 and L3 with focal lengths f_2 = 500 mm and f_3 = 150 mm, respectively, formed an image of the plane conjugated to the SLM display in the plane of the lens L4 with a focal length f_4 = 150 mm. The intensity distributions of the investigated laser beams formed at various distances from the plane of the lens L4 were captured with a video camera CAM (TOUPCAM UHCCD00800KPA, 3264 × 2448 pixels) mounted on the optical rail.

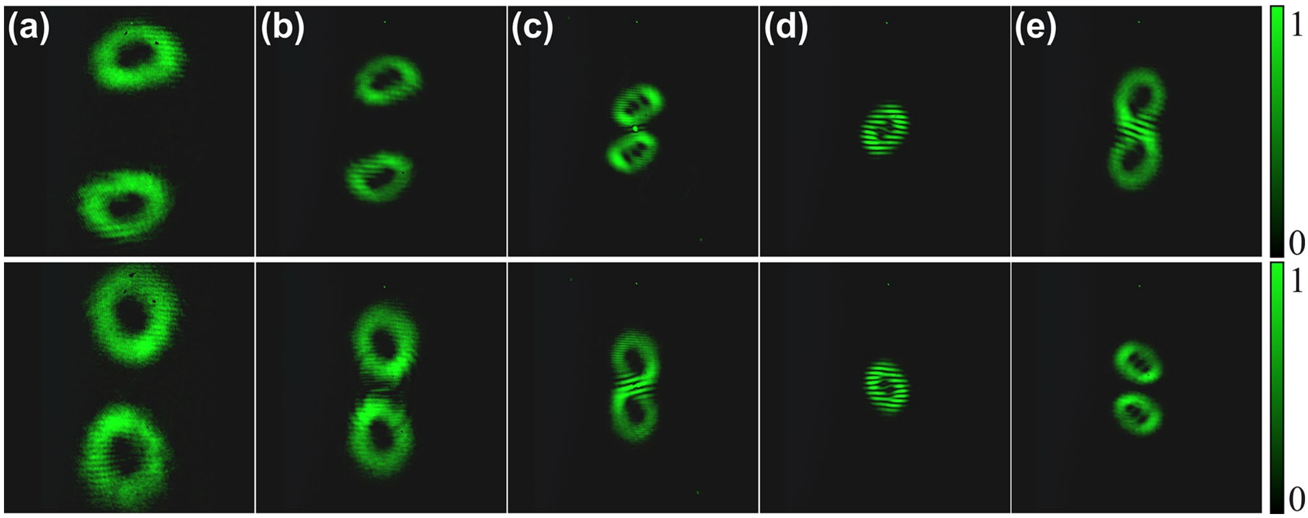

Fig. 10 The intensity distributions of laser beams formed in the case of a couple of shifted vortex LG beams $(n, m) = (0, 3)$ at different distances from the plane of the lens L4: **a** *f*—50 mm, **b** *f*—25 mm, **c** the focal plane, *f*, **d** *f* + 50 mm, **e** *f* + 50 mm. The top row shows the distributions for sublinear chirp ($q = 1$, $\alpha = 0.0025$), the bottom row—for superlinear chirp ($q = 3$, $\alpha = 0.0033$)

The experimentally obtained results for numerically investigated laser beams are shown in Figs. 8, 9 and 10. Figure 8 shows intensity distributions formed in the case of the triple of two-mode LG beams with Ω: $(n_1, m_1) = (0, 1)$, $(n_2, m_2) = (0, 2)$ according to simulations results of Fig. 3. Figure 9 shows intensity distributions formed in the case of clusters of superposition LG beams according to simulations results of Fig. 3. Figure 10 shows intensity distributions formed in the case of a couple of shifted vortex LG beams $(n, m) = (0, 3)$ according to simulations results of Fig. 5.

All experimental results are in good agreement with the numerically obtained results.

5 Conclusion

We investigated theoretically, numerically and experimentally generation of clusters of beams which are LG beams superpositions with individual deflecting phase (spatial carriers). The possibility of forming autofocusing beams when not only clusters rotating as a whole, but also ensuring the rotation of their individual components is shown. This provides complex 3D propagation scenarios which expands the range of beams used for optical trapping and manipulation of microparticles.

We have considered another approach to control the autofocusing trajectory and astigmatic transformation cluster's beams based on the introduction of a common phase function with a power-law dependence on the radius. It is shown that for $1 \le q < 2$ (sublinear chirp) and $q > 2$ (superlinear chirp) the nature of the astigmatic transformation before and after the focusing plane is different. In this case, astigmatic intensity patterns, which make it possible to unambiguously determine the TC of the beam, are most clearly observed for $q = 1$ before the focal plane and for $q = 3$ after the focal plane.

For experimental generation of structured light beams clusters with autofocusing properties and astigmatic-like transformation, we used SLMs. It should be noted that the SLM application makes it possible to dynamically control the 3D structure of the formed beams by changing both the propagation trajectory and the distribution of the transverse intensity of each cluster element during propagation.

The proposed techniques provide additional control of the three-dimensional trajectories of the structured laser beams with predetermined intensity and phase distributions. Such types of laser beams can be used for laser guiding of optically-trapped particles, including the laser guiding of microparticles along curves around various obstacles [7–9], for laser fabrication of three-dimensional microstructures inside an isotropic polymer materials [4, 5], and for precisely measuring the single-molecule localization and orientation [78–80].

Author contributions SNK performed theoretical analysis and numerical simulation, APP conducted experimental realization. SNK and APP wrote the main manuscript text and reviewed the manuscript.

Funding This work was financially supported by the Russian Science Foundation (grant No. 22-12-00041) in part of theoretical and numerical results and by the Ministry of Science and Higher Education within the State assignment FSRC «Crystallography and Photonics» RAS (No. 007-GZ/Ch3363/26) in part of experimental investigations.

Data availability The data generated and analysed during the current study are available from the corresponding author on reasonable request.

Declarations

Conflict of interest The authors declare no conflict of interests.

References

1. J.A. Neff, R.A. Athale, S.H. Lee, Two-dimensional spatial light modulators: a tutorial. Proc. IEEE **78**(5), 826–855 (1990). https://doi.org/10.1109/5.53402
2. J.P. Huignard, Spatial light modulators and their applications. J. Opt. **18**(4), 181 (1987). https://doi.org/10.1088/0150-536X/18/4/003
3. Z. Kuang, W. Perrie, J. Leach, M. Sharp, S.P. Edwardson, M. Padgett, G. Dearden, K.G. Watkins, High throughput diffractive multi-beam femtosecond laser processing using a spatial light modulator. Appl. Surf. Sci. **255**(5:1), 2284–2289 (2008). https://doi.org/10.1016/j.apsusc.2008.07.091
4. J. Ni, C. Wang, C. Zhang, Y. Hu, L. Yang, Z. Lao, B. Xu, J. Li, D. Wu, J. Chu, Three-dimensional chiral microstructures fabricated by structured optical vortices in isotropic material. Light Sci. Appl. **6**(7), e17011 (2017). https://doi.org/10.1038/lsa.2017.11
5. P.S. Salter, M.J. Booth, Adaptive optics in laser processing. Light Sci. Appl. **8**, 110 (2019). https://doi.org/10.1038/s41377-019-0215-1
6. A.P. Porfirev, S.N. Khonina, N.A. Ivliev, A. Meshalkin, E.A. Achimova, A. Forbes, Writing and reading with the longitudinal component of light using carbazole-containing azopolymer thin films. Sci. Rep. **12**, 3477 (2022). https://doi.org/10.1038/s41598-022-07440-9
7. J. Liesener, M. Reicherter, T. Haist, H.J. Tiziani, Multi-functional optical tweezers using computer-generated holograms. Opt. Commun. **185**(1–3), 77–82 (2000). https://doi.org/10.1016/S0030-4018(00)00990-1
8. M. Woerdemann, C. Alpmann, M. Esseling, C. Denz, Advanced optical trapping by complex beam shaping. Laser Photon. Rev. **7**(6), 839–854 (2013). https://doi.org/10.1002/lpor.201200058
9. J.A. Rodrigo, T. Alieva, Freestyle 3D laser traps: tools for studying light-driven particle dynamics and beyond. Optica **2**(9), 812–815 (2015). https://doi.org/10.1364/OPTICA.2.000812
10. Z. Wang, N. Zhang, X.-C. Yuan, High-volume optical vortex multiplexing and de-multiplexing for free-space optical communication. Opt. Express **19**(2), 482–492 (2011). https://doi.org/10.1364/OE.19.000482
11. J. Wang, Advances in communications using optical vortices. Photonics Res. **4**(5), B14–B28 (2016). https://doi.org/10.1364/PRJ.4.000B14
12. S.N. Khonina, S.V. Karpeev, M.A. Butt, Spatial-light-modulator-based multichannel data transmission by vortex beams of various orders. Sensors **21**(9), 2988 (2021). https://doi.org/10.3390/s21092988
13. A.Y.M. Ng, C.W. See, M.G. Somekh, Quantitative optical microscope with enhanced resolution using a pixelated liquid crystal spatial light modulator. J. Microsc. **214**(3), 334–340 (2004). https://doi.org/10.1111/j.0022-2720.2004.01323.x
14. C. Maurer, A. Jesacher, S. Bernet, M. Ritsch-Marte, What spatial light modulators can do for optical microscopy. Laser Photonics Rev. **5**(1), 81–101 (2011). https://doi.org/10.1002/lpor.200900047
15. M. Aakhte, E.A. Akhlaghi, H. Müller, J. Arno, SSPIM: a beam shaping toolbox for structured selective plane illumination microscopy. Sci. Rep. **8**, 10067 (2018). https://doi.org/10.1038/s41598-018-28389-8
16. T.-H. Tsai, X. Yuan, D.J. Brady, Spatial light modulator based color polarization imaging. Opt. Express **23**(9), 11912–11926 (2015). https://doi.org/10.1364/OE.23.011912
17. S. Mukherjee, A. Vijayakumar, J. Rosen, Spatial light modulator aided noninvasive imaging through scattering layers. Sci. Rep. **9**, 17670 (2019). https://doi.org/10.1038/s41598-019-54048-7
18. D. Pierangeli, G. Marcucci, C. Conti, Large-scale photonic Ising machine by spatial light modulation. Phys. Rev. Lett. **122**(21), 213902 (2019). https://doi.org/10.1103/PhysRevLett.122.213902
19. J.A. Davis, D.E. McNamara, D.M. Cottrell, T. Sonehara, Two-dimensional polarization encoding with a phase-only liquid crystal spatial light modulator. Appl. Opt. **39**(10), 1549–1554 (2000). https://doi.org/10.1364/AO.39.001549
20. I. Moreno, J.A. Davis, T.M. Hernandez, D.M. Cottrell, D. Sand, Complete polarization control of light from a liquid crystal spatial light modulator. Opt. Express **20**(1), 364–376 (2012). https://doi.org/10.1364/OE.20.000364
21. S.N. Khonina, A.V. Ustinov, A.P. Porfirev, Vector Lissajous laser beams. Opt. Lett. **45**(15), 4112–4115 (2020). https://doi.org/10.1364/OL.398209
22. L. Zhu, J. Wang, Arbitrary manipulation of spatial amplitude and phase using phase-only spatial light modulators. Sci. Rep. **4**(1), 7441 (2014). https://doi.org/10.1038/srep07441
23. R.W. Gerchberg, W.O. Saxton, A practical algorithm for the determination of the phase from image and diffraction plane pictures. Optik **35**(2), 237–246 (1972)
24. C.-Y. Chen, W.-C. Li, H.-T. Chang, C.-H. Chuang, T.-J. Chang, 3-D modified Gerchberg-Saxton algorithm developed for panoramic computer-generated phase-only holographic display. J. Opt. Soc. Am. B **34**(5), B42–B48 (2017). https://doi.org/10.1364/JOSAB.34.000B42
25. T. Zhao, Y. Chi, Modified Gerchberg-Saxton (G-S) algorithm and its application. Entropy **22**(12), 1354 (2020). https://doi.org/10.3390/e22121354
26. J.A. Davis, E.D. Wolfe, I. Moreno, D.M. Cottrell, Encoding complex amplitude information onto phase-only diffractive optical elements using binary phase Nyquist gratings. OSA Continuum **4**(3), 896–910 (2021). https://doi.org/10.1364/OSAC.418578
27. C. Maurer, A. Jesacher, S. Fürhapter, S. Bernet, M. Ritsch-Marte, Tailoring of arbitrary optical vector beams. New J. Phys. **9**(3), 78 (2007). https://doi.org/10.1088/1367-2630/9/3/078
28. S.N. Khonina, A.P. Porfirev, Harnessing of inhomogeneously polarized Hermite-Gaussian vector beams to manage the 3D spin angular momentum density distribution. Nanophotonics **11**(4), 697–712 (2022). https://doi.org/10.1515/nanoph-2021-0418
29. N.K. Efremidis, D.N. Christodoulides, Abruptly autofocusing waves. Opt. Lett. **35**(23), 4045–4047 (2010).
30. I. Chremmos, N.K. Efremidis, D.N. Christodoulides, Pre-engineered abruptly autofocusing beams. Opt. Lett. **36**(10), 1890–1892 (2011). https://doi.org/10.1364/OL.36.001890
31. J.A. Davis, D.M. Cottrell, D. Sand, Abruptly autofocusing vortex beams. Opt. Express **20**(12), 13302–13310 (2012). https://doi.org/10.1364/OE.20.013302
32. P. Zhang, J. Prakash, Z. Zhang, M.S. Mills, N.K. Efremidis, D.N. Christodoulides, Z. Chen, Trapping and guiding microparticles with morphing autofocusing Airy beams. Opt. Lett. **36**(15), 2883–2885 (2011). https://doi.org/10.1364/OL.36.002883
33. Y. Jiang, K. Huang, X. Lu, Radiation force of abruptly autofocusing Airy beams on a Rayleigh particle. Opt. Express **21**(20), 24413–24421 (2013). https://doi.org/10.1364/OE.21.024413
34. M. Manousidaki, D.G. Papazoglou, M. Farsari, S. Tzortzakis, Abruptly autofocusing beams enable advanced multiscale

photo-polymerization. Optica **3**(5), 525–530 (2016). https://doi.org/10.1364/OPTICA.3.000525
35. P. Panagiotopoulos, D.G. Papazoglou, A. Couairon, S. Tzortzakis, Sharply autofocused ring-Airy beams transforming into non-linear intense light bullets. Nat. Commun. **4**, 2622 (2013). https://doi.org/10.1038/ncomms3622
36. S. Liu, M. Wang, P. Li, P. Zhang, J. Zhao, Abrupt polarization transition of vector autofocusing Airy beams. Opt. Lett. **38**(14), 2416–2418 (2013). https://doi.org/10.1364/OL.38.002416
37. S.A. Degtyarev, S.G. Volotovsky, S.N. Khonina, Sublinearly chirped metalenses for forming abruptly autofocusing cylindrically polarized beams. J. Opt. Soc. Am. B **35**(8), 1963–1969 (2018). https://doi.org/10.1364/JOSAB.35.001963
38. G.A. Siviloglou, D.N. Christodoulides, Accelerating finite energy Airy beams. Opt. Lett. **32**(8), 979–981 (2007). https://doi.org/10.1364/OL.32.000979
39. A.A. Kovalev, V.V. Kotlyar, S.G. Zaskanov, Structurally stable three-dimensional and two-dimensional laser half Pearcey beams. Comput. Opt. **38**(2), 193–197 (2014). https://doi.org/10.18287/0134-2452-2014-38-2-193-197
40. F. Zang, Y. Wang, L. Li, Dual self-accelerating properties of one-dimensional finite energy Pearcey beam. Results Phys. **15**, 102656 (2019). https://doi.org/10.1016/j.rinp.2019.102656
41. T. Poston, I. Steward, *Catastrophe theory and its applications* (Pitman Publishing Limited, 1978)
42. R. Gilmore, *Catastrophe theory for scientists and engineers* (Wiley and Sons, New York, 1981)
43. AYu. Kravtsov, Yu.I. Orlov, Caustics, catastrophes, and wave fields. Sov. Phys. Usp. **26**, 1038–1058 (1983). https://doi.org/10.1070/PU1983v026n12ABEH004582
44. P. Vaveliuk, A. Lencina, J.A. Rodrigo, O.M. Matos, Caustics, catastrophes, and symmetries in curved beams. Phys. Rev. A **92**(3), 033850 (2015). https://doi.org/10.1103/PhysRevA.92.033850
45. J. Ring, J. Lindberg, A. Mourka, M. Mazilu, K. Dholakia, M. Dennis, Auto-focusing and self-healing of Pearcey beams. Opt. Express **20**(17), 18955–18966 (2012). https://doi.org/10.1364/OE.20.018955
46. X. Chen, D. Deng, J. Zhuang, X. Yang, H. Liu, G. Wang, Non-paraxial propagation of abruptly autofocusing circular Pearcey Gaussian beams. Appl. Opt. **57**(28), 8418–8423 (2018). https://doi.org/10.1364/AO.57.008418
47. C. Sun, D. Deng, G. Wang, X. Yang, W. Hong, Abruptly autofocusing properties of radially polarized circle Pearcey vortex beams. Opt. Commun. **457**, 124690 (2020). https://doi.org/10.1016/j.optcom.2019.124690
48. S.N. Khonina, Mirror and circular symmetry of autofocusing beams. Symmetry **13**(10), 1794 (2021). https://doi.org/10.3390/sym13101794
49. P. Li, S. Liu, T. Peng, G. Xie, X. Gan, J. Zhao, Spiral autofocusing Airy beams carrying power-exponent phase vortices. Opt. Express **22**(7), 7598–7606 (2014). https://doi.org/10.1364/OE.22.007598
50. Y. Zhang, P. Li, S. Liu, L. Han, H. Cheng, J. Zhao, Manipulating spin-dependent splitting of vector abruptly autofocusing beam by encoding cosine-azimuthal variant phases. Opt. Express **24**(25), 28409–28418 (2016). https://doi.org/10.1364/OE.24.028409
51. S.N. Khonina, A.V. Ustinov, A.P. Porfirev, Aberration laser beams with autofocusing properties. Appl. Opt. **57**(6), 1410–1416 (2018). https://doi.org/10.1364/AO.57.001410
52. A. Brimis, K.G. Makris, D.G. Papazoglou, Tornado waves. Opt. Lett. **45**(2), 280–283 (2020). https://doi.org/10.1364/OL.45.000280
53. B. Lü, H. Ma, Beam propagation properties of radial laser arrays. J. Opt. Soc. Am. A **17**(11), 2005–2009 (2000). https://doi.org/10.1364/JOSAA.17.002005
54. Y. Izdebskaya, V. Shvedov, A. Volyar, Symmetric array of off-axis singular beams: spiral beams and their critical points. J. Opt. Soc. Am. A **25**(1), 171–181 (2008). https://doi.org/10.1364/JOSAA.25.000171
55. R.A. Suarez, A.A. Neves, M.R. Gesualdi, Generation and characterization of an array of Airy-vortex beams. Opt. Commun. **458**, 124846 (2019). https://doi.org/10.1016/j.optcom.2019.124846
56. L. Song, Z. Yang, S. Zhang, X. Li, Dynamics of rotating Laguerre-Gaussian soliton arrays. Opt. Express **27**(19), 26331–26345 (2019). https://doi.org/10.1364/OE.27.026331
57. J. Turunen, A. Vasara, A.T. Friberg, Holographic generation of diffraction-free beams. Appl. Opt. **27**(19), 3959–3962 (1988). https://doi.org/10.1364/AO.27.003959
58. Z. Zhai, Z. Cheng, Q. Lv, X. Wang, Tunable axicons generated by spatial light modulator with high-level phase computer generated holograms. Appl. Sci. **10**(15), 5127 (2020). https://doi.org/10.3390/app10155127
59. S.N. Khonina, N.L. Kazanskiy, P.A. Khorin, M.A. Butt, Modern types of axicons: new functions and applications. Sensors **21**(19), 6690 (2021). https://doi.org/10.3390/s21196690
60. I. Amidror, The Fourier-spectrum of circular sine and cosine gratings with arbitrary radial phases. Opt. Commun. **149**(1–3), 127–134 (1998). https://doi.org/10.1016/S0030-4018(98)80006-0
61. S. Hasegawa, H. Ito, H. Toyoda, Y. Hayasaki, Diffraction-limited ring beam generated by radial grating. OSA Continuum **1**(2), 283–294 (2018). https://doi.org/10.1364/OSAC.1.000283
62. S. Zheng, J. Wang, Measuring orbital angular momentum (OAM) states of vortex beams with annular gratings. Sci. Rep. **7**, 40781 (2017). https://doi.org/10.1038/srep40781
63. L. Allen, M.W. Beijersbergen, R. Spreeuw, J. Woerdman, Orbital angular momentum of light and the transformation of Laguerre-Gaussian laser modes. Phys. Rev. A **45**(11), 8185–8189 (1992). https://doi.org/10.1103/PhysRevA.45.8185
64. A. O'Neil, I. MacVicar, L. Allen, M. Padgett, Intrinsic and extrinsic nature of the orbital angular momentum of a light beam. Phys. Rev. Lett. **88**(5), 053601 (2002). https://doi.org/10.1103/PhysRevLett.88.053601
65. V. Namias, The fractional Fourier transform and its application in quantum mechanics. JIMA **25**(3), 241–265 (1980). https://doi.org/10.1093/imamat/25.3.241
66. S. Abe, J.T. Sheridant, Generalization of the fractional Fourier transformation to an arbitrary linear lossless transformation: an operator approach. J. Phys. A Math. Gen. **27**(12), 4179–4187 (1994). https://doi.org/10.1088/0305-4470/27/12/023
67. T. Alieva, M.J. Bastiaans, M.L. Calvo, Fractional transforms in optical information processing. EURASIP J. Adv. Signal Process. **2005**, 1498–1519 (2005). https://doi.org/10.1155/ASP.2005.1498
68. D. Mendlovic, H.M. Ozaktas, Fractional Fourier transformations and their optical implementation: I. J. Opt. Soc. Am. A **10**(9), 1875–1881 (1993). https://doi.org/10.1364/JOSAA.10.001875
69. J.N. McMullin, The ABCD matrix in arbitrarily tapered quadratic-index waveguides. Appl. Opt. **25**(13), 2184–2184 (1986). https://doi.org/10.1364/AO.25.002184
70. D.Q. Lu, W. Hu, Y.J. Zheng, Y.B. Liang, L.G. Cao, S. Lan, Q. Guo, Self-induced fractional Fourier transform and revivable higher-order spatial solitons in strongly nonlocal nonlinear media. Phys. Rev. A **78**(4), 043815 (2008). https://doi.org/10.1103/PhysRevA.78.043815
71. Z.P. Dai, Z.J. Yang, S.M. Zhang, Z.G. Pang, Propagation of anomalous vortex beams in strongly nonlocal nonlinear media. Opt. Commun. **350**, 19–27 (2015). https://doi.org/10.1016/j.optcom.2015.03.071
72. A.P. Prudnikov, Yu.A. Brychkov, O.I. Marichev, *Integrals and series. Volume 2: special functions* (CRC Press, 1986)

73. H. Kogelnik, T. Li, Laser beams and resonators. Appl. Opt. **5**(10), 1550–1567 (1966). https://doi.org/10.1364/AO.5.001550
74. E.G. Abramochkin, T. Alieva, J.A. Rodrigo, Solutions of paraxial equations and families of Gaussian beams, in *Mathematical optics: classical, quantum, and computational methods*. ed. by V. Lakshmianrayanan, M.L. Calvo, T. Alieva (CRC Press, Boca Raton, 2013), pp.143–192
75. E. Abramochkin, V. Volostnikov, Spiral-type beams. Opt. Commun. **102**(3–4), 336–350 (1993). https://doi.org/10.1016/0030-4018(93)90406-U
76. V.V. Kotlyar, V.A. Soifer, S.N. Khonina, Rotation of multimode Gauss-Laguerre light beams in free space. Tech. Phys. Lett. **23**(9), 657–658 (1997). https://doi.org/10.1134/1.1261648
77. S.N. Khonina, A.P. Porfirev, A.V. Ustinov, Sudden autofocusing of superlinear chirp beams. J. Opt. **20**(2), 025605 (2018). https://doi.org/10.1088/2040-8986/aaa075
78. G.J. Schütz, M. Axmann, H. Schindler, Imaging single molecules in three dimensions. Sing. Mol. **2**, 69–74 (2001)
79. S.R.P. Pavani, R. Piestun, Three dimensional tracking of fluorescent microparticles using a photon-limited double-helix response system. Opt. Express **16**(26), 22048–22057 (2008)
80. V. Anand, S. Khonina, R. Kumar, N. Dubey, A.N.K. Reddy, J. Rosen, S. Juodkazis, Three-dimensional incoherent imaging using spiral rotating point spread functions created by double-helix beams [Invited]. Nanoscale Res. Lett. **17**, 37 (2022). https://doi.org/10.1186/s11671-022-03676-6
81. M.W. Beijersbergen, L. Allen, H.E.L.O. van der Veen, J.P. Woerdman, Astigmatic laser mode converters and transfer of orbital angular momentum. Opt. Commun. **96**(1–3), 123–132 (1993). https://doi.org/10.1016/0030-4018(93)90535-D
82. V.V. Kotlyar, A.A. Kovalev, A.P. Porfirev, Astigmatic transforms of an optical vortex for measurement of its topological charge. Appl. Opt. **56**(14), 4095–4104 (2017). https://doi.org/10.1364/AO.56.004095
83. S.A. Goorden, J. Bertolotti, A.P. Mosk, Superpixel-based spatial amplitude and phase modulation using a digital micromirror device. Opt. Express **22**(15), 17999–18009 (2014). https://doi.org/10.1364/OE.22.017999